

Molecular dynamics simulation of thermal transport at a nanometer scale constriction in silicon

Sanjoy K. Saha and Li Shi^{a)}

Department of Mechanical Engineering, The University of Texas at Austin, Austin, Texas 78712, and Center for Nano and Molecular Science and Technology, Texas Materials Institute, The University of Texas at Austin, Austin, Texas 78712

(Received 13 August 2006; accepted 26 January 2007; published online 10 April 2007)

To better understand thermal transport at nanoscale point contacts such as the tip-sample contact of a scanning probe microscope and at the contact between a nanotube and a planar surface, we have used a nonequilibrium molecular dynamics (MD) method to calculate the temperature distribution and thermal resistance of a nanometer scale constriction formed between two planar silicon substrates of different temperatures. Surface reconstruction was observed at the two free silicon surfaces and at the constriction. The radius of the heated zone in the cold substrate was found to approach a limit of about 20 times the average nearest-neighbor distance of boron doping atoms when the constriction radius (a) is reduced below the interdopant distance. The phonon mean free path at the constriction was found to be suppressed by diffuse phonon-surface scattering and phonon-impurity scattering. The MD thermal resistance is close to the ballistic resistance when a is larger than 1 nm, suggesting that surface reconstruction does not reduce the phonon transmission coefficient significantly. When a is 0.5 nm and comparable to the dominant phonon wavelength, however, the MD result is considerably lower than the calculated ballistic resistance because bulk phonon dispersion and bulk potential are no longer accurate. The MD thermal resistance of the constriction increases slightly with increasing doping concentration due to the increase in the diffusive resistance. © 2007 American Institute of Physics. [DOI: 10.1063/1.2715488]

I. INTRODUCTION

Thermal transport across nanometer scale point constrictions plays an important role in a number of technologies. Such constrictions can be found in the tip-sample contacts of scanning probe microscopes as well as in the application of carbon nanotubes as thermal interface materials. Recently, Lyeo *et al.*¹ reported an ultrahigh vacuum (UHV) scanning thermoelectric microscopy method (S_{Th}EM) for probing the local Seebeck coefficient (S) of nanostructured thermoelectric materials. In the measurement, an atomically sharp metal tip makes a nanometer size contact on a heated III-V semiconductor sample, creating a large temperature gradient possibly of the order of 10^{10} K/m at the contact. The local temperature gradient causes carrier diffusion and results in a thermoelectric voltage that is proportional to the local Seebeck coefficient of the nonuniform temperature zone. The size of the resulting nonuniform temperature zone in the semiconductor determines the spatial resolution of the measurement, which appears to be about two times the average nearest-neighbor interdopant distance of 4–10 nm in the doped GaAs samples and is smaller than the bulk phonon mean free path. This finding is intriguing, since a temperature gradient cannot be established within a region smaller than the phonon mean free path.

In a related effort, the superhigh thermal conductivity of carbon nanotubes has inspired several experimental efforts where carbon nanotubes (CNTs) are employed as thermal

interface materials for electronic packaging.^{2,3} An intriguing question on these efforts is concerned with a potentially high thermal resistance at the nanometer point contacts between a CNT and a planar surface.

There have been extensive theoretical studies of the thermal resistance of a point contact between two solid materials.^{4,5} Two expressions of thermal resistance at a point constriction can be obtained, one for the macroscopic diffusive resistance at Maxwell's limit where the radius of the constriction (a) is much larger than the phonon mean free path (l) in the bulk material, i.e., the Knudsen number $K \equiv l/a \ll 1$, and another for the ballistic resistance at the Knudsen limit of $K \gg 1$. Wexler unified these two limiting cases and introduced a single equation for the thermal resistance of an orifice by adding up the diffusive resistance (R_d) and ballistic resistance (R_b),⁶

$$R = \gamma(K)R_d + R_b, \quad (1)$$

where $\gamma(K)$ is a slowly varying function with $\gamma(0)=1$ and $\gamma(\infty)=0.694$. The diffusive resistance is calculated to be⁴

$$R_d = 1/2ka, \quad (2)$$

where k is the thermal conductivity.

The ballistic thermal resistance can be calculated as follows.^{7–11} By integrating the ballistic phonon flux from different directions through a constriction or orifice with radius a much smaller than l , one can obtain the net heat current transferred through the orifice as

^{a)}Author to whom correspondence should be addressed; electronic mail: lishi@mail.utexas.edu

$$q = \frac{\pi a^2}{4} \Delta T \int_{\omega=0}^{\infty} v_g \frac{\partial \langle n_0 \rangle}{\partial T} D(\omega) \hbar \omega d\omega, \quad (3)$$

where ΔT is the temperature difference between the phonons immediately at the two sides of the constriction, v_g is the phonon group velocity, $\langle n_0 \rangle$ is the occupation of phonons given by the Bose-Einstein distribution corresponding to the local equilibrium temperature T , $D(\omega)$ is the phonon density of states at frequency ω , and \hbar is Planck's constant. The ballistic thermal resistance is obtained as

$$R_b \equiv \frac{\Delta T}{q} = \left[\frac{\pi a^2}{4} \int_{\omega=0}^{\infty} v_g \frac{\partial \langle n_0 \rangle}{\partial T} D(\omega) \hbar \omega d\omega \right]^{-1}. \quad (4)$$

For the case that the phonon group velocity is independent of frequency, Eq. (4) is reduced to

$$R_b = 4/(Cv_g \pi a^2). \quad (5)$$

If the phonon mean free path is also independent of frequency, Eq. (5) can be further expressed according to the thermal conductivity expression $k = Cv_g l/3$ to be

$$R_b = 4l/(3\pi k a^2) = 4K/(3\pi k a). \quad (6)$$

It is assumed in this analytical model that the deviation from the equilibrium distribution is small. This assumption is inappropriate for SThEM and other nanoscale point contacts, where large nonequilibrium prevails locally at the contact point. Moreover, Eq. (4) assumes complete phonon transmission at the constriction. This is a limiting case because atomic reconstruction can occur in a realistic constriction, potentially reducing the phonon transmission coefficient. When the constriction size is smaller than the dominant phonon wavelength (λ_0), Rayleigh scattering of phonons can also reduce the transmission coefficient according to Prasher *et al.*¹² Furthermore, the temperature distribution at the constriction is not given by this model.

To better understand thermal transport at nanoscale constrictions, here we report a theoretical study of highly non-equilibrium thermal transport at a nanoscale constriction in silicon using nonequilibrium (NE) molecular dynamics (MD) simulation. The simulation method and results are discussed in the following sections.

II. SIMULATION METHOD

We have used a NEMD method to simulate thermal transport across a circular constriction formed between two Si (100) substrates, as shown in Fig. 1. The simulation box is a cube, for which the length in each of the three dimensions is 200 nm. There are about 400×10^6 atoms in the cube. Atoms were arranged in diamond lattice structure and the simulation box coincides with the [100], [010], and [001] directions. The simulation box has been divided into two parts. The top half and the bottom half represent two Si substrates with their (100) surfaces facing each other. At the interface of the two Si substrates, there is a phonon blocking partition with a small circular constriction or orifice at the center that allows phonon transport between the two parts. It is assumed that except at the central constriction the surface atoms at one side of the phonon blocking partition do not

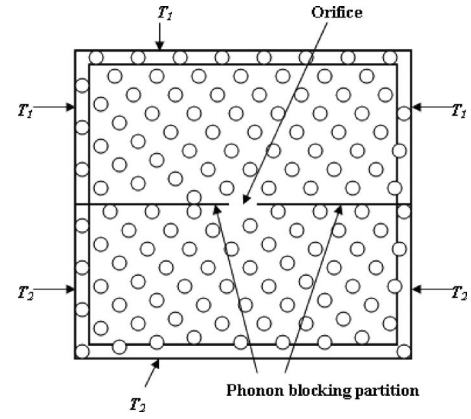


FIG. 1. Schematic diagram of the simulation box. The initial temperature is 300 K. $T_1 = 340$ K and $T_2 = 300$ K.

have force interaction with the atoms at the other surface. The two surfaces at the two sides of the partition are thus equivalent to two free surfaces facing each other without any energy transfer between them except at the constriction. In the simulation, the outer walls of the top part are maintained at temperature T_1 , and the outer walls of the lower part are maintained at a different temperature T_2 .

Because the electron contribution to heat conduction in silicon is small, an atomistic model such as the MD method that ignores electron transport is appropriate for the current problem. Further, a MD simulation can deal with highly non-equilibrium situations and can reveal atomic reconstruction at the surfaces. For this reason, this approach is appropriate for the problem of nanoscale constrictions and interfaces.

Because one of our objectives is to find the temperature profile at the nanoconstriction, we have used the direct method that relies on imposing a temperature gradient across the simulation cell,¹³⁻¹⁵ instead of the Green-Kubo approach,^{16,17} which is an equilibrium MD method that uses current fluctuations to compute the thermal conductivity via the fluctuation-dissipation theorem.

A potential for solid Si has been formulated by Stillinger and Weber (SW).¹⁸ The SW potential utilizes two and three body interaction terms to stabilize the diamond lattice that consists of atoms held in place by strong and directional bonds. The reduced pair potentials are described as follows:

$$f_2(r) = \begin{cases} A(Br^{-p} - r^{-q}) \exp[(r-a)^{-1}], & r < a \\ 0, & r \geq a, \end{cases} \quad (7)$$

where r is the distance between atoms, a is the cutoff radius, and A , B , p , and q are fitting parameters. This generic form automatically cuts off at $r = a$ without discontinuities in any r derivatives. The three body interaction term is written as

$$f_3(r_i, r_j, r_k) = f_{3a}(r_{ij}, r_{ik}, \theta_{jik}) + f_{3b}(r_{ji}, r_{jk}, \theta_{ijk}) + f_{3c}(r_{ki}, r_{kj}, \theta_{ikj}) \quad (8)$$

where

$$f_{3a}(r_{ij}, r_{ik}, \theta_{jik}) = \begin{cases} \lambda \exp[\gamma(r_{ij}-a)^{-1} + \gamma(r_{ik}-a)^{-1}](\cos \theta_{jik} + 1/3)^2, & r_{ij} \text{ and } r_{ik} < a \\ 0, & r_{ij} \text{ and } r_{ik} > a. \end{cases} \quad (9)$$

The term f_{3a} vanishes for $\theta_{jik} = \cos^{-1}(-1/3)$, favoring ideal tetrahedral bond. In these formulas, r is the distance between two atoms and θ_{jik} is the angle at the vertex at particle i of the triplet. The parameter values are $A=7.049$, $B=0.602$, $p=4$, $q=0$, $\lambda=21.0$, and $\gamma=1.2$. At the phonon blocking partition, the potential between the two (100) Si substrates is switched off and the two substrates interact with each other through SW potential only at the central constriction. Except at the constriction, the two surfaces at the two sides of the partition are treated as two free surfaces following the method by Volz and Chen.¹⁷ The integration method used for our molecular dynamics simulation is the predictor-corrector method.¹⁹

We have investigated the case of uniform boron doping in the entire simulation box because boron is a common doping element in Si. Particles designated as dopants differ from silicon atoms in both the atomic mass and their interactions with their neighbors. In order to introduce some mismatch, the values of potential parameters A and B are changed to values that lead to an increase in the interatomic spacing between silicon and boron. Hence, the location of potential minima will be shifted to a slightly larger atomic spacing. Only substitutional doping atoms were considered in this work. Although interatomic spacing between a substitutional boron atom and a neighboring silicon atom is larger than that between two neighboring silicon atoms, the diamond lattice structure remains the same. Consequently, the three body potential that stabilizes the diamond lattice structure is the same for silicon and impurity. Following Kelly and Ungar,²⁰ we have chosen values for A and B as $A=8.535$ and $B=0.80$ for the impurity atoms. The location of the potential minimum for these parameters is about 2.45 Å, as compared to 2.35 Å for silicon-silicon interaction. The mass of the impurity atom is taken to be the atomic mass of boron.

To implement the isothermal wall condition for the outer walls of the computation box shown in Fig. 1, we have employed the method of Maiti *et al.*¹³ For the constant temperature boundary condition, the heat current at the boundary is calculated as follows:^{21,22}

$$q(t) = \left(\sum_{i=1}^N v_i \tilde{E}_i + \sum_{i=1}^N \sum_{j=1}^N F_{ij} v_i r_{ij} \right) / V, \quad (10)$$

where $q(t)$ is the instantaneous heat current, F_{ij} is the force, r_{ij} is the distance between the i th and j th particle, and V is the volume. \tilde{E}_i is the total excess energy defined by

$$\tilde{E}_i = \sum_j f_2(r_{ij}) + \sum_j \sum_k f_3(r_{ij}, r_{jk}, r_{ki}, \theta_{ijk}, \theta_{jki}, \theta_{kij}) + \frac{1}{2} m_i v_i^2 - h_i, \quad (11)$$

where h_i is the enthalpy of the i th atom, $f_2(r_{ij})$ is the pair potential energy, and $f_3(r_{ij}, r_{jk}, r_{ki}, \theta_{ijk}, \theta_{jki}, \theta_{kij})$ is the three body potential.

When a temperature gradient is applied in the NEMD simulation, the center of mass of the entire system tends to drift.¹⁵ The drift can result in an inaccurate measurement of the actual local temperature. We have used the velocity-rescaling algorithm of Jund and Jullien that eliminates the drift.¹⁵ According to this algorithm the modified velocity at each iteration is given by

$$v'_i = v_G + \alpha(v_i - v_G), \quad (12)$$

where v_G is the velocity of the center of mass of the ensemble of atoms in the domain selected for velocity rescaling and

$$\alpha = \sqrt{1 \pm \frac{\Delta \varepsilon}{E_c^R}}. \quad (13)$$

The + (or -) sign in Eq. (13) applies to the case when the atoms are in the domain where heat is added (or removed). For the constant temperature boundary condition, $\Delta \varepsilon$ is the difference in the total kinetic energy of the atoms in the domain before and after the constant temperature boundary condition is maintained. The relative kinetic energy E_c^R is given by

$$E_c^R = \frac{1}{2} \sum_i m_i v_i^2 - \frac{1}{2} \sum_i m_i v_G^2. \quad (14)$$

For this direct MD method, it is important to establish a steady-state heat current flow. This amounts to obtaining a stationary temperature profile as a function of time, thus insuring that only a steady-state current is allowed. It was found by Maiti *et al.*¹³ that long simulations of about 1×10^{-9} s were necessary to achieve a smooth temperature profile for a Si grain boundary system.

In this work, we found that a steady-state heat current was obtained for a total simulation time of 1.1×10^{-9} s, or 2×10^6 MD steps with each MD time step being 0.55×10^{-15} s, as discussed in the following. We used a grid system to divide the simulation box, with each grid volume consisting of about 49 atoms. The average temperature of the atoms in each grid was calculated. The averaging was performed over a large number of MD steps according to

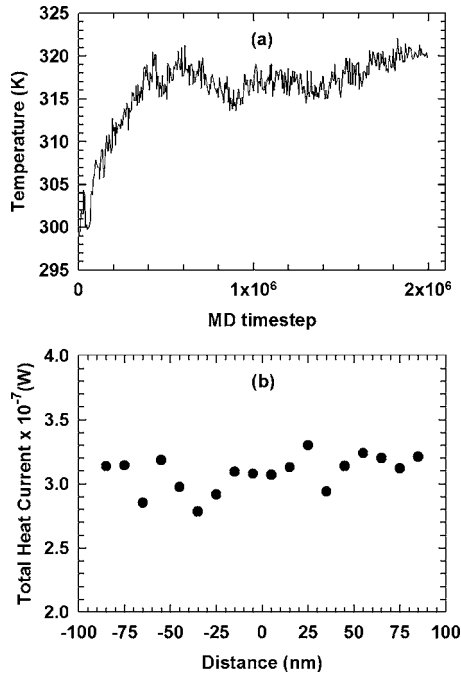


FIG. 2. (a) Time-averaged temperature of the grid space at the center of the constriction for a constriction radius of 2 nm and doping concentration of $3 \times 10^{20} \text{ cm}^{-3}$. (b) Time-averaged total heat current across the boundaries of rectangular boxes at different vertical distances or depths measured from the constriction. The width of the box is twice the depth.

$$\frac{1}{M} \sum_{j=0}^{M-1} \sum_{i=1}^n m v_i^2 = \frac{3}{2} \frac{n}{N_{\text{tot}}} \int \langle n_0 \rangle \hbar \omega D(\omega) d\omega, \quad (15)$$

where M is the number of steps on which the averaging is performed, m is the mass of the silicon atom, v_i is the velocity of the i th atom, n is the number of atoms in the cell, and N_{tot} is the total number of atoms in the simulation. Phonon dispersion for bulk silicon based on the Stillinger-Weber potential was used in the right-hand side of Eq. (15), and the temperature contained in the $\langle n_0 \rangle$ term is solved numerically from Eq. (15).²³ Here, although the MD simulation treats the vibrating atoms as classical particles, the total kinetic energy of the system is mapped onto the appropriate phonon distribution function $\langle n_0 \rangle$ according to Eq. (15) in order to correctly define the temperature. A common practice of defining the temperature using the formula $\frac{1}{2} \sum_i m v_i^2 = \frac{3}{2} n k_B T$ would be erroneous for the current problem as the temperature of interest is much lower than the Debye temperature of silicon.

The total number of steps in the simulation is N , and thus M must be smaller than $N-1$. For small M , the fluctuations in the obtained time-averaged temperature are entirely statistical and not due to transient effects related to the heat current sources. As M increases, fluctuations due to transient effects may be observed. Figure 2(a) shows the time-averaged temperature of the grid space at the center of the constriction for a 200 nm size box and a doping concentration of $3 \times 10^{20} \text{ cm}^{-3}$. Each temperature point in the curve was the averaged value for 5000 MD steps. The averaging eliminates large temperature fluctuation. As shown in Fig. 2(a), the system achieves steady state after about 1×10^6 MD steps. Hence, 2×10^6 MD steps is sufficiently long for ob-

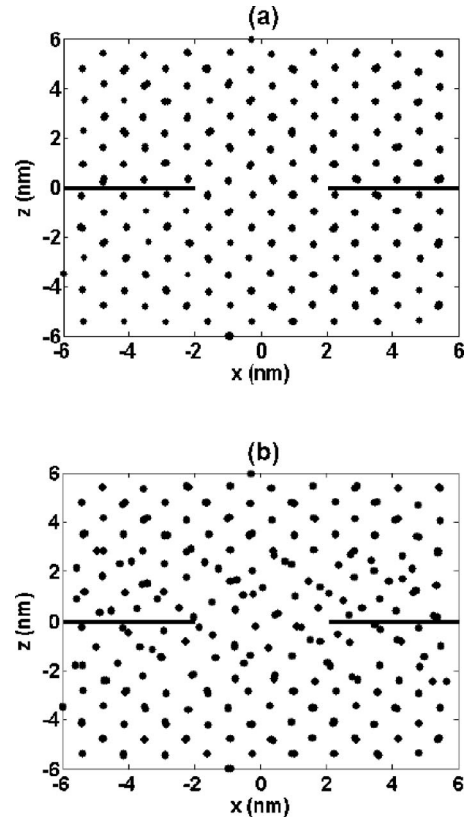


FIG. 3. Two-dimensional projection of atoms in a 2 nm deep, 12 nm high, and 12 nm wide box centered at the constriction (a) at the beginning and (b) at the completion of the simulation.

taining the time-averaged temperature profile and steady-state heat current. Because of the large number (400×10^6) of atoms in the simulation box, it took about 30 days for each simulation that was run in dedicated LINUX computer clusters to achieve steady state.

At both sides of the partition, the heat current across the outer walls of rectangular boxes of different vertical depths measured from the constriction was calculated. The width of the rectangular boxes is twice the depth. The heat current was calculated for each individual grid cell on the outer walls of the rectangular box and added up to obtain the total heat current across the outer walls. The heat current calculation for each cell was based on Eq. (10) and was averaged over the last 8×10^5 steps. As shown in Fig. 2(b), the difference between the total heat current across boxes of different depths is within 10%. The average value of all the heat current data calculated for different depths was used for thermal resistance calculation.

Figures 3(a) and 3(b) show the two-dimensional (2D) projection of the atoms inside a 2 nm thick, 12 nm high, 12 nm wide rectangular box centered at the constriction at the beginning and at the completion of the simulation, respectively. The atoms are positioned in a diamond lattice structure in Fig. 3(a), whereas in Fig. 3(b) the surface atoms become disordered, indicating that surface reconstruction occurs as the simulation proceeds. The reconstruction occurs mainly within 2 nm distance from the two free surfaces at the partition. Because of the reconstruction, the two free surfaces become rough. The roughness can lead to diffuse phonon-surface scattering.

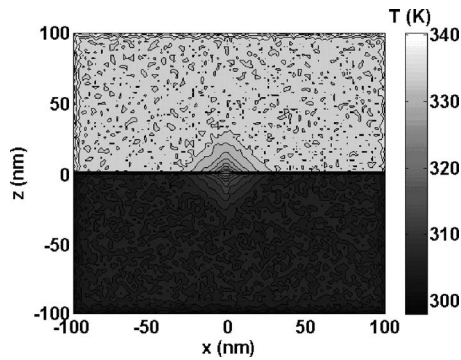


FIG. 4. Temperature distribution on the vertical section passing through the center of the constriction with a constriction radius of 2 nm and a boron doping concentration of $3 \times 10^{20}/\text{cm}^3$.

As a benchmark experiment to check the correctness of the MD code, we have modified the code according to the procedure of Schelling *et al.* to calculate the thermal conductivity of solid Si.¹⁴ The calculated thermal conductivities at $T=155, 255,$ and 300 K are 322, 163, and 119 W/m K, respectively, in agreement with the simulation results of Schelling *et al.* and the measurement results in the literature.^{14,24}

III. SIMULATION RESULTS AND DISCUSSIONS

The temperature profile on the vertical plane passing through the center of the constriction is plotted in Fig. 4, where the doping concentration is $N_d=3 \times 10^{20}$ at./ cm^3 . To compute the time-averaged spatial temperature distribution, we have used the results for the final 8×10^5 MD steps and have left out the data for the initial 1.2×10^6 MD steps. This procedure ensures that we have allowed sufficient time so that the system can reach steady state and the result does not consist of any transient effects.

Figure 5 shows the temperature profile along the vertical axis passing the center point of the constriction. There is a temperature drop of about 28 K at the constriction and a drop of about 6 K each at the upper and lower walls of the simulation box. The temperature drops at the boundary are believed to be an artifact caused by enforced phonon scattering at the heat source and sink.^{13,14} There is a flat temperature region between the outer boundaries and the constriction, indicating that the artifacts due to the enforced phonon-

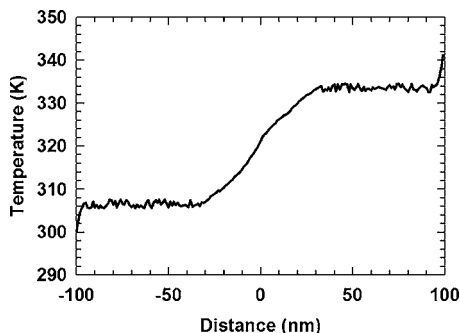


FIG. 5. Temperature profile along the vertical axis passing the center of the constriction as a function of the distance from the constriction. The constriction radius is 2 nm. The doping concentration is $N_d=3 \times 10^{20} \text{ cm}^{-3}$.

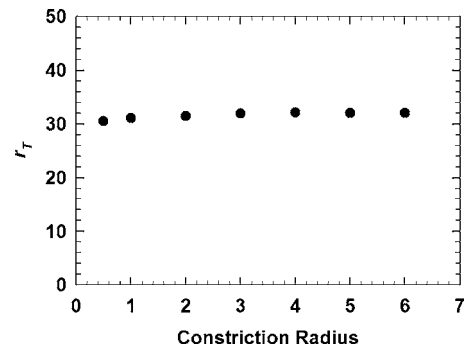


FIG. 6. r_T as a function of a for $N_d=3 \times 10^{20}/\text{cm}^3$ corresponding to $d=1.5$ nm.

boundary scattering at the outer boundaries diminish in this flat temperature region as well as near the constriction. We have used the temperature drop across the constriction and between the two flat temperature regions for calculating the thermal resistance, thus eliminating the influence of the heat source or sink effect at the outer boundaries. Moreover, reducing the simulation box from 200 to 120 nm in each dimension would not change the temperature profile and temperature drop across the constriction. Hence, the 200 nm size simulation box is large enough to impose the isothermal boundary condition at the outer walls.

A. Effect of the constriction radius

We have examined the effect of the constriction radius (a) on the temperature distribution and thermal resistance of the constriction. We calculated the radius of the heated zone in the cold substrate as the distance (r_T) on the vertical axis from the center of the constriction for which $\Delta T(r_T)=T(r_T)-T_2=0.1(T_1-T_2)$. The resulting value of $\Delta T(r_T)$ is 4 K, which is small enough compared to T_1-T_2 and just slightly larger than the statistical precision of the simulation of about 2 K. Figure 6 shows the calculated r_T as a function of the constriction radius (a) in the range between 0.5 and 6 nm, for doping concentration of 3×10^{20} at./ cm^3 . The calculated r_T decreases rather slowly with decreasing a to approach about 20 times of the average nearest-neighbor inter dopant distance (d) that is estimated to be $d=(1/N_d)^{1/3}=1.5$ nm, where N_d is the number density of impurity dopants. Because the smallest length scale within which thermal equilibrium can be obtained cannot be smaller than the phonon mean free path (l), r_T cannot be shorter than l when a is reduced below l . Hence, l at the constriction cannot be longer than $20d$ or 30 nm.

We have calculated the bulk phonon mean free path (l) using a procedure where the phonon dispersion is taken into account.^{25,26} At room temperature, about one-third of the specific heat of Si is due to optical phonons. Since optical phonons have a very low group velocity, their contribution to the bulk thermal conductivity is negligible and one only needs to calculate the mean free path for the acoustic phonons based on the kinetic theory $k=Cvl/3$, where k , C , v , and l are the thermal conductivity, specific heat, group velocity, and mean free path, respectively, of the acoustic phonons. In addition to excluding the optical phonons, we

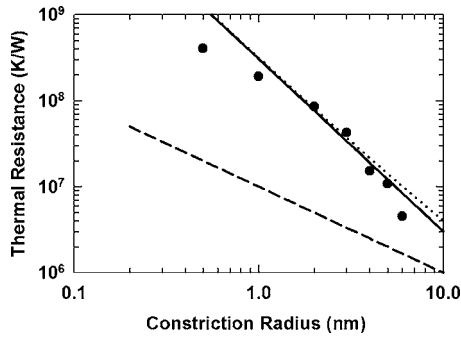


FIG. 7. The MD thermal resistance (filled circles) as a function of constriction radius (a) for $N_d=3 \times 10^{20}/\text{cm}^3$. Also plotted are R_b (solid black line) based on Eq. (4), R_d (dashed black line) from Eq. (2) with the use of the bulk k , and the total thermal resistance R (dotted line) calculated using Eqs. (1), (2), and (4).

calculated the phonon group velocity from the phonon dispersion weighed over the relative contribution to the specific heat. Based on the calculation we obtained the heat capacity and group velocity of acoustic phonons at room temperature as $C=0.93 \times 10^6 \text{ J/m}^3 \text{ K}$ and $v=1804 \text{ m/s}$. Using the experimental value of thermal conductivity for bulk silicon at the doping concentration of $3 \times 10^{20}/\text{cm}$, $k=50 \text{ W/m K}$,^{25–27} we calculated the bulk phonon mean free path to be $l=89 \text{ nm}$.

The obtained bulk l is about three times that of r_T , which cannot be shorter than l at the constriction according to the above discussion. This discrepancy is attributed to a shorter l at the constriction than in the bulk. The shorter l is caused by frequent diffuse phonon scattering at the roughened free surface and phonon-impurity scattering at the vicinity of the constriction. Due to the interplay of these two scattering processes, phonons are scattered for multiple times by both the partition and impurity atoms before they escape the constriction. The short l in the vicinity of the constriction also explains that the diffuse outer walls do not introduce artifacts in the calculation results even when the bulk l is close to the vertical depth of the top or bottom part of the simulation box.

The thermal resistances of the constriction were calculated for a doping concentration of $3 \times 10^{20}/\text{cm}^3$ and different constriction radii, as shown in Fig. 7. In the MD simulation, the thermal resistance is calculated as $R=\Delta T/q$. Here, q is the total heat current calculated according to the above discussion and ΔT is the temperature drop at the constriction between the two flat temperature regions so that the temperature drops at the upper and lower walls of the simulation box are excluded from ΔT .

Figure 7 also shows the total thermal resistance R calculated using Eqs. (1), (2), and (4). Here, $\gamma(K)$ is calculated following Wexler.⁶ Also plotted are the ballistic resistance R_b calculated from Eq. (4) and the diffusive resistance from Eq. (2). The Knudsen numbers corresponding to the constriction radius are larger than 9, well within the Knudsen limit, so that the obtained thermal resistance from Eq. (1) mainly comes from the ballistic resistance R_b from Eq. (4). The MD results were found to be close to R_b when the constriction radius is larger than 1 nm, indicating that surface reconstruction does not reduce the phonon transmission coefficient sig-

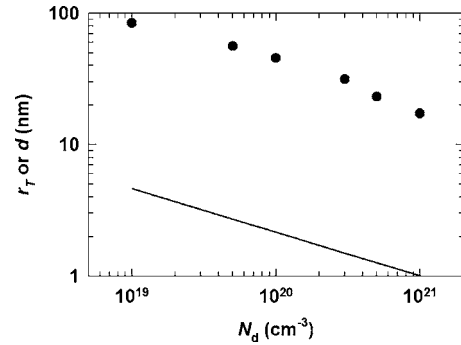


FIG. 8. r_T (open circles) and d (solid line) as a function of N_d for $a=2 \text{ nm}$.

nificantly. At $a=0.5 \text{ nm}$, however, the MD result is considerably lower than R_b . The discrepancy is attributed to the fact that bulk phonon dispersion and the SW potential are no longer accurate at the constriction when a is reduced to be comparable to or smaller than the dominant phonon wavelength, which is about 1 nm in Si at 300 K.

B. Effect of the doping concentration

We have investigated the effect of the concentration of boron concentration N_d on r_T . N_d was varied from 10^{19} to 10^{21} cm^{-3} with a fixed $a=2 \text{ nm}$. Figure 8 shows r_T together with the interdopant distance d as a function of N_d . At this constriction radius, r_T decreases with increasing doping concentration and is about $20d$. This feature manifests the interplay between diffuse phonon-surface scattering by the free surface and phonon-impurity scattering at the constriction. The observation of decreasing r_T with increasing doping concentration explains why the spatial resolution of SThEM was found to improve with increasing doping concentration in the experiment of Lyeo *et al.*¹ The lack of alloy scattering in Si could have led to the larger l and r_T at the Si constriction considered here than in the III-V constriction in the experiment of Lyeo *et al.* Nevertheless, the simulation result supports the experimental observation that the spatial resolution of SThEM and thus r_T can be smaller than the bulk phonon mean free path.

Figure 9 shows that the MD thermal resistance of the constriction increases slightly with N_d . Also shown in Fig. 9

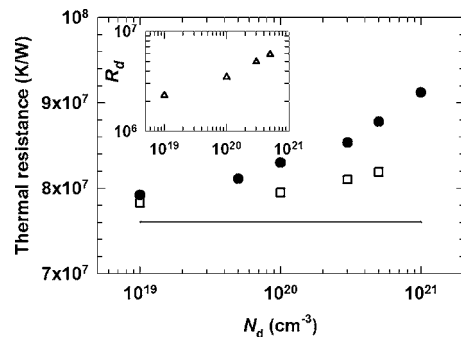


FIG. 9. MD thermal resistance (filled circles) of the constriction as a function of N_d for $a=2 \text{ nm}$. Also shown are R_b (line) from Eq. (4) and the total thermal resistance R (open squares) calculated using Eqs. (1), (2), and (4) with the use of the bulk k . The inset shows the obtained R_d from Eq. (2) with the use of bulk k .

are the total thermal resistance R calculated using Eqs. (1), (2), and (4), where the bulk k was used, and the ballistic resistance R_b from Eq. (4). The diffusive resistance R_d based on Eq. (2) is shown in the inset of the figure. For the calculation of R_d , k of bulk silicon at different doping concentrations was taken from literature.^{27,28} It can be expected that doping has a much smaller effect on the phonon dispersion, specific heat, and group velocity that determine R_b than on l that affects k and R_d . Consequently, the increase in the thermal resistance with N_d should be mainly caused by the increase in R_d . In the calculation of R_b from Eq. (4) (as well as in the MD simulation), the phonon dispersion is assumed to be independent of the doping concentration, resulting in the constant R_b shown in Fig. 9 at different N_d . Note that the MD data increase more rapidly with N_d than the total resistance R from Eq. (1), although the amounts of increase are on the same order of magnitude. The use of the bulk k , which is larger than the effective k of the constriction, can underestimate R_d and yield the slower increase of the total resistance R with doping concentration.

IV. CONCLUSIONS

The MD calculation reveals several phenomena that are not shown by the analytical model. Most notably, the radius of the heated zone in the cold substrate was found to approach a limit of 20 times the average nearest-neighbor distance of impurity doping atoms when the constriction radius is reduced below the interdopant distance. The phonon mean free path at the constriction was found to be suppressed by diffuse phonon-boundary scattering and phonon-impurity scattering. When the constriction radius is larger than 1 nm, the MD thermal resistances of the constriction are close to the ballistic thermal resistance, suggesting that surface reconstruction does not reduce the phonon transmission coefficient at the constriction significantly. When the constriction radius is 0.5 nm, however, the MD result is considerably lower than the ballistic resistance calculated based on bulk phonon dispersion. This discrepancy is attributed to the fact that bulk phonon dispersion and SW potential are no longer accurate at a constriction with radius comparable to or smaller than the dominant phonon wavelength. The MD resistance increases slightly with increasing doping concentration due to the increase in the diffusive resistance. These results can help to better understand thermal transport at the tip-sample con-

tacts of various scanning probe microscopy methods and at the point contacts between a nanotube and a planar surface.

ACKNOWLEDGMENTS

This work is supported in part by the National Science Foundation (Thermal Systems Program) and Office of Naval Research Contract No. N00014-04-1-0532 (Program manager: Dr. Mihal E. Gross). The authors thank Intel Higher Education Program for the donation of workstations that were used for this research and Professor Gang Chen and Dr. Ravi S. Prasher for helpful discussions.

- ¹H. K. Lyeo, A. A. Khajetoorians, L. Shi, K. P. Pipe, R. J. Ram, A. Shakouri, and C. K. Shih, *Science* **303**, 816 (2004).
- ²H. F. Chuang, S. M. Cooper, M. Meyyappan, and B. A. Cruden, *J. Nanosci. Nanotechnol.* **4**, 964 (2004).
- ³Q. Ngo, B. A. Cruden, A. M. Cassell, G. Sims, M. Meyyappan, J. Li, and C. Y. Yang, *Nano Lett.* **4**, 2403 (2004).
- ⁴C. V. Madhusudana, *Thermal Contact Conductance* (Springer-Verlag, New York, 1996), pp. 1–43.
- ⁵M. G. Cooper, B. B. Mikic, and M. M. Yovanovich, *Int. J. Heat Mass Transfer* **12**, 279 (1968).
- ⁶G. Wexler, *Proc. Phys. Soc. London* **89**, 927 (1966).
- ⁷Y. V. Sharvin, *Sov. Phys. JETP* **21**, 655 (1965).
- ⁸L. Weber, E. Gmelin, and H. J. Queisser, *Phys. Rev. B* **40**, 1244 (1989).
- ⁹W. A. Little, *Can. J. Phys.* **37**, 334 (1959).
- ¹⁰B. Nikolic and P. B. Allen, *Phys. Rev. B* **60**, 3963 (1999).
- ¹¹R. S. Prasher, *Nano Lett.* **5**, 2155 (2005).
- ¹²R. S. Prasher, T. Tao, and A. Majumdar, *Proceedings of International Mechanical Engineering Congress and Exposition, IMECE2006-15592*, 2006 (unpublished).
- ¹³A. Maiti, G. D. Mahan, and S. T. Pantelides, *Solid State Commun.* **102**, 517 (1997).
- ¹⁴P. K. Schelling, S. R. Phillpot, and P. Keblinski, *Phys. Rev. B* **65**, 144306 (2002).
- ¹⁵P. Jund and R. Jullien, *Phys. Rev. B* **59**, 13707 (1999).
- ¹⁶J. Che, T. Cagin, W. Deng, and W. A. Goddard, *J. Chem. Phys.* **113**, 6888 (2000).
- ¹⁷S. G. Volz and G. Chen, *Appl. Phys. Lett.* **75**, 2056 (1999).
- ¹⁸F. H. Stillinger and T. A. Weber, *Phys. Rev. B* **31**, 5262 (1985).
- ¹⁹D. C. Rapaport, *The Art of Molecular Dynamics Simulation* (Cambridge University Press, Cambridge, England, 2004).
- ²⁰F. X. Kelly and L. H. Ungar, *J. Cryst. Growth* **102**, 658 (1990).
- ²¹P. Bhattacharya, S. K. Saha, A. Yadav, P. Phelan, and R. S. Prasher, *J. Appl. Phys.* **95**, 6492 (2004).
- ²²Y. H. Lee, R. Biswas, C. M. Soukoulis, C. Z. Wang, C. T. Chan, and K. M. Ho, *Phys. Rev. B* **43**, 6573 (1991).
- ²³X.-P. Li, G. Chen, P. B. Allen, and J. Q. Broughton, *Phys. Rev. B* **38**, 3331 (1988).
- ²⁴C. J. Glassbrenner and G. A. Slack, *Phys. Rev.* **134**, A1058 (1964).
- ²⁵G. Chen, *Phys. Rev. B* **57**, 14958 (1998).
- ²⁶G. Chen, *J. Heat Transfer* **119**, 220 (1997).
- ²⁷G. A. Slack, *J. Appl. Phys.* **35**, 3460 (1964).
- ²⁸M. Asheghi, K. Kurabayashi, K. Kasnavi, and K. E. Goodson, *J. Appl. Phys.* **91**, 5079 (2002).